

General Lossless Spatial Polarization Transformations

Alicia Sit,¹ Lambert Giner,^{1,*} Ebrahim Karimi,^{1,2} and Jeff S. Lundeen¹

¹ Physics Department, Centre for Research in Photonics, University of Ottawa, Advanced Research Complex, 25 Templeton, Ottawa ON Canada, K1N 6N5

² Department of Physics, Institute for Advanced Studies in Basic Sciences, 45137-66731 Zanjan, Iran

E-mail: *lginer@uottawa.ca

Abstract. Liquid crystals allow for the real-time control of the polarization of light. We describe and provide some experimental examples of the types of general polarization transformations, including universal polarization transformations, that can be accomplished with liquid crystals in tandem with fixed waveplates. Implementing these transformations with an array of liquid crystals, e.g., a spatial light modulator, allows for the manipulation of the polarization across a beam's transverse plane. We outline applications of such general spatial polarization transformations in the generation of exotic types of vector polarized beams, a polarization magnifier, and the correction of polarization aberrations in light fields.

Keyword : Polarization, Liquid-crystal devices, Quantum information and processing

1. Introduction

For the last century, polarization manipulation has mostly been conducted using birefringent crystals, known as waveplates, by physically rotating them about a light beam's propagation axis [1, 2, 3, 4, 5]. However, waveplates manipulate the polarization uniformly across a beam's transverse profile; that is, they do not allow for spatially varying polarization manipulation. A cell of uniformly aligned liquid crystals acts as a waveplate with a fixed orientation optical axis and a voltage-controlled variable birefringence. When arranged in an array, such as in a liquid-crystal spatial light modulators (LC-SLM), these devices can spatially tailor the polarization distribution of light by individually controlling the voltage across each cell.

LC-SLMs are widely used for dynamic generation of optical beams possessing particular intensity and phase profile [6, 7, 8]. In the past fifteen years, their inherent birefringence has been used to produce arbitrary spatially polarized beams. However, the schemes to do so are inherently lossy; they rely on spatial and polarization filtering [9, 10, 11, 12, 13, 14, 15, 16, 17, 18, 19]. While with classical optics and photonic communications this signal loss is undesirable, in quantum optics it can completely destroy the quantum nature of the light being acted on [20].

Consequently, the polarization transformation schemes that we present, like the schemes in Refs. [21, 22, 23, 24, 25, 26], do not require optical loss in order to function. Whereas all of these references focus solely on generating spatially-varying polarized states of light, we additionally investigate the implementation of general spatial polarization transformations. Implementing these would enable unprecedented control over spatially-varying polarization distributions. Such control could have applications in studying the dynamics and topologies of polarization vortices [27, 28, 29, 30, 31], creating exotic polarization topologies in beams, e.g., a Möbius strip in polarization [32], creating novel optical traps for biology and atomic physics [12, 33], for optically guiding and pumping microfluids [34, 35], and for micro-machining [36, 37, 38]. In the quantum realm, spatially polarized states can be used to multiply communication bandwidth through superdense coding [39, 40], perform tests of fundamental quantum physics [41, 42], implement quantum key distribution [43, 44, 45], and for building measurement devices with quantum-enhanced sensitivities [46, 47].

We limit ourselves to light fields that are perfectly polarized at each spatial point and to transformations that maintain this perfect degree of polarization. Moreover, the transformations should not involve loss, at least in principle. These are known as unitary transformations and are mathematically enacted by Jones Matrices [48]. In turn, these are equivalent to rotations in the Poincaré sphere, as we will review in Section 2 and use throughout this paper. In Section 3, we will discuss three different kinds of universal unitaries that can be created by combining voltage-controlled liquid crystal cells and fixed waveplates: 1. Variable phase retardation of a fixed but arbitrary polarization. 2. Transformation from an arbitrary polarization state to another arbitrary polarization state. 3. Variable retardation of a variable arbitrary polarization state. At the expense of requiring increasing numbers of waveplates and liquid crystal devices, going from the first to last, these transformations increase in generality. The latter is the most general unitary possible for polarization transformations.

The mathematical theory underlying these transformations has not been previously presented. The paper provides explicit formulae and the underlying

definitions and conventions that are needed to implement these general polarization transformations in practice. Moreover, the distinct goals of arbitrary polarization generation and arbitrary transformations are often conflated. We clarify the fundamental differences between them and show that have different requirements and constraints.

2. Background theory

2.1. Waveplates and liquid crystal cells

In this section, we describe the transformation of polarization by birefringent media in terms of rotations in the Poincaré sphere. Since many mutually inconsistent polarization conventions exist in the literature, we give a brief introduction and review of polarization transformations in Appendix A, which sets the conventions and notation used in this paper. Light passing through birefringent media, such as a waveplate, gains a phase between the electric field component along the media's optical axis and the orthogonal component. This phase is known as the “retardance,” Δ . On the Poincaré sphere, the action of a waveplate corresponds to a rotation of an input polarization $\hat{\mathbf{s}}$ by Δ about a rotation axis $\hat{\mathbf{k}}(2\Phi, 0)$, i.e., one lying in the $\hat{\mathbf{s}}_1\hat{\mathbf{s}}_2$ plane at 2Φ from the positive $\hat{\mathbf{s}}_1$ axis. Here, Φ is the angle in the laboratory between the fast axis and horizontal, $\hat{\mathbf{x}}$, with increasing angle defined to be towards $\hat{\mathbf{y}}$. Accordingly, waveplates, such as half-wave plates ($\Delta = \pi$, HWP) and quarter-wave plates ($\Delta = \pi/2$, QWP), can be described by a rotation matrix. More generally, a birefringent waveplate with arbitrary retardance Δ (e.g., an electro-optic modulator (EOM) or a nematic-phase parallel-aligned liquid crystal) will have the rotation matrix [50],

$$\mathbf{R}_{\mathbf{k}(2\Phi,0)}(\Delta) = \begin{bmatrix} \sin^2 2\Phi \cos \Delta + \cos^2 2\Phi & \sin^2 \left(\frac{\Delta}{2}\right) \sin 4\Phi & \sin 2\Phi \sin \Delta \\ \sin^2 \left(\frac{\Delta}{2}\right) \sin 4\Phi & \cos^2 2\Phi \cos \Delta + \sin^2 2\Phi & -\cos 2\Phi \sin \Delta \\ -\sin 2\Phi \sin \Delta & \cos 2\Phi \sin \Delta & \cos \Delta \end{bmatrix}. \quad (1)$$

Since we will be using HWP and QWPs frequently, we define $\mathbf{HWP}[\Phi] \equiv \mathbf{R}_{\mathbf{k}(2\Phi,0)}(\pi)$ and $\mathbf{QWP}[\Phi] \equiv \mathbf{R}_{\mathbf{k}(2\Phi,0)}(\pi/2)$. To avoid any confusion between the reference frames the angles are defined in, an angle expressed the laboratory frame is written using $[\cdot]$.

In the Poincaré sphere, an arbitrary general polarization transformation $\mathbf{R}_{\mathbf{k}}(\xi)$ consists of a rotation about an arbitrary axis $\hat{\mathbf{k}}$ by angle ξ (i.e., Eq. (25)). One can implement this with half- and quarter-wave plates cascaded in the following sequence:

$$\mathbf{R}_{\mathbf{k}}(\xi) = \mathbf{QWP}[\Phi_3]\mathbf{HWP}[\Phi_2]\mathbf{QWP}[\Phi_1]. \quad (2)$$

Ordered first to last, the waveplates the light passes through respectively correspond to the elements in Eq. (2) from right to left. By an appropriate rotation of each of the three waveplates in the laboratory, any unitary polarization transformation can be created [2]. However, this mechanical rotation will prohibit fast changes of the unitary polarization transformation.

Now suppose we had a birefringent optical element with retardance Δ and rotation axis $\hat{\mathbf{k}}_A$, and we wished to convert $\hat{\mathbf{k}}_A$ to be $\hat{\mathbf{k}}_B$, as in Fig. 2(a). This could be done by sandwiching the optical element between two sequences of Eq. (2),

$$\begin{aligned} \mathbf{R}_{\hat{\mathbf{k}}_B}(\Delta) = & \text{QWP}[\Phi_1 + 90^\circ] \text{HWP}[\Phi_2 + 90^\circ] \text{QWP}[\Phi_3 + 90^\circ] \\ & \cdot \mathbf{R}_{\hat{\mathbf{k}}_A}(\Delta) \text{QWP}[\Phi_3] \text{HWP}[\Phi_2] \text{QWP}[\Phi_1], \end{aligned} \quad (3)$$

where $\mathbf{R}_{\hat{\mathbf{k}}_A}(\Delta)$ is the corresponding rotation matrix of the birefringent optical element, and again, light passes through the elements from right to left. The first sequence of quarter- and half-wave plates rotates the polarization state $\hat{\mathbf{s}}_B$ (positioned at $\hat{\mathbf{k}}_B$ on the sphere) to $\hat{\mathbf{s}}_A$ (positioned at $\hat{\mathbf{k}}_A$). The second sequence applies the reverse rotation, rotating it back to $\hat{\mathbf{s}}_B$. In essence, this is a change of basis such that $\hat{\mathbf{s}}_B$, a polarization eigenstate of $\mathbf{R}_{\hat{\mathbf{k}}_B}(\Delta)$, is unaffected by the waveplates and optical elements — apart from a global phase — and all other polarization states undergo a rotation by Δ about $\hat{\mathbf{k}}_B$.

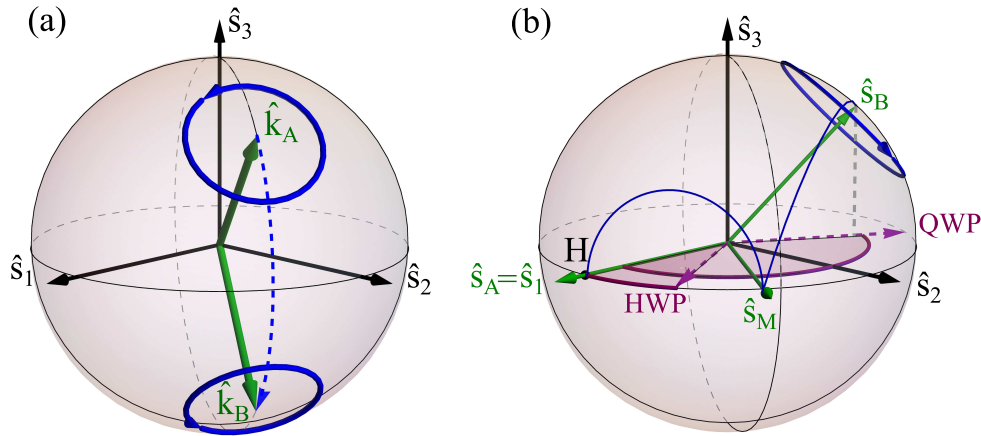


Figure 1: (a) Representation on the Poincaré Sphere of the transformation of an arbitrary rotation axis $\hat{\mathbf{k}}_A$ into another one $\hat{\mathbf{k}}_B$. To perform such a transformation, a sequence of three waveplates (QWP→HWP→QWP) converts $\hat{\mathbf{k}}_A$ into $\hat{\mathbf{k}}_B$. (b) For a fixed liquid crystal to perform a rotation about an arbitrary axis $\hat{\mathbf{k}}_B$, one needs to convert the crystal's rotation axis, $\hat{\mathbf{k}}_A$ to $\hat{\mathbf{k}}_B$ (we take $\hat{\mathbf{k}}_A = \hat{\mathbf{s}}_1$). Consider the passage of state $\hat{\mathbf{s}}_B = \hat{\mathbf{k}}_B$ through the sequence of waveplates. First a QWP removes the ellipticity of $\hat{\mathbf{s}}_B$, transforming it into $\hat{\mathbf{s}}_M$, which lies on the equator of the sphere. Then, a HWP rotates $\hat{\mathbf{s}}_M$ to $\hat{\mathbf{s}}_A = \hat{\mathbf{s}}_1 = \hat{\mathbf{k}}_A$, the eigenbasis of the LC-SLM. A general polarization state will be rotated by $\Delta(x, y)$ around $\hat{\mathbf{s}}_1$, here. To finish, $\hat{\mathbf{s}}_A$ is converted back to $\hat{\mathbf{s}}_B$ using the inverse transformation that had converted it from $\hat{\mathbf{s}}_B$ to $\hat{\mathbf{s}}_A$.

Liquid crystals in the nematic phase and which are parallel-aligned have variable retardances, but a fixed rotation axis $\hat{\mathbf{k}}(2\Phi, 0)$ in the $\hat{\mathbf{s}}_1\hat{\mathbf{s}}_2$ plane. Since they have a fixed axis with linear polarization eigenstates, fewer waveplates are necessary in Eq. (3): only a quarter- and half-wave plate are required to transform any linear polarization to an arbitrary polarization state [1]. Consequently, a four waveplate combination is sufficient for a liquid crystal cell to effectively create an arbitrary

rotation $\mathbf{R}_{\mathbf{k}_B(\varphi,\theta)}(\Delta)$,

$$\begin{aligned} \mathbf{R}_{\mathbf{k}_B(\varphi,\theta)}(\Delta) = & \mathbf{QWP} \left[\left[\frac{\varphi}{2} + 90^\circ \right] \right] \mathbf{HWP} \left[\left[\frac{\varphi - \theta}{4} + \frac{\Phi}{2} + 90^\circ \right] \right] \\ & \cdot \mathbf{R}_{\mathbf{k}(2\Phi,0)}(\Delta) \mathbf{HWP} \left[\left[\frac{\varphi - \theta}{4} + \frac{\Phi}{2} \right] \right] \mathbf{QWP} \left[\left[\frac{\varphi}{2} \right] \right]. \end{aligned} \quad (4)$$

The action of the waveplates in Eq. (4) is shown in Fig. 1(b) for $\hat{\mathbf{k}}(2\Phi,0) = \hat{\mathbf{s}}_1$. We will repeatedly use this method of converting rotation axes on the Poincaré sphere in the following sections.

3. General polarization transformations with spatial light modulators

3.1. Spatially variable rotation about a fixed axis

If many liquid crystal cells are arranged in an array, we obtain a spatial light modulator (LC-SLM). Here, for simplicity, we take the fast axis of each liquid crystal cell, and thus the whole LC-SLM, to be along the horizontal. i.e., with $\Phi = 0$. If one used uniformly H polarized light, a nematic-phase parallel aligned LC-SLM would function as it is commonly used: as a “phase-only” spatial light modulator. Here, we consider other input polarizations. The LC-SLM has a rotation matrix equivalent to Eq. (28) but with a spatially variable retardance (or “phase distribution”) of $\Delta(x,y)$. In this way, LC-SLMs provide the spatial degree of freedom to extend the general polarization transformation in Eq. (4) to be,

$$\begin{aligned} \mathbf{R}_{\mathbf{k}_B(\varphi,\theta)}(\Delta(x,y)) = & \\ \mathbf{QWP} \left[\left[\frac{\varphi}{2} + 90^\circ \right] \right] \mathbf{HWP} \left[\left[\frac{\varphi - \theta}{4} + 90^\circ \right] \right] \mathbf{SLM}(\Delta(x,y)) \mathbf{HWP} \left[\left[\frac{\varphi - \theta}{4} \right] \right] \mathbf{QWP} \left[\left[\frac{\varphi}{2} \right] \right]. \end{aligned} \quad (5)$$

The corresponding rotation matrix can then be computed by using Eq. (1) for the quarter- and half-wave plates, and Eq. (28) for the LC-SLM. This configuration gives the possibility for the whole LC-SLM to have an arbitrary fixed rotation axis $\hat{\mathbf{k}}_B(\varphi,\theta)$, but with a spatially variable rotation angle $\Delta(x,y)$. Fig. 1(b) traces the path of a state $\hat{\mathbf{s}}_B = \hat{\mathbf{k}}_B$ on the Poincaré Sphere as it travels through the waveplates in Eq. (5).

3.2. Practical examples and special cases

Let us look at some practical examples of Eq. (5).

(i) For a rotation axis on the equator (i.e., $\hat{\mathbf{s}}_1\hat{\mathbf{s}}_2$ plane), the quarter-wave plates in Eq. (5) can be removed, and $\varphi = 0$. For example, for rotations about $\hat{\mathbf{k}}_B = \hat{\mathbf{s}}_2$, the diagonal polarization axis, the sequence would be $\mathbf{R}_{\mathbf{s}_2}(\Delta(x,y)) = \mathbf{HWP} [112.5^\circ] \mathbf{SLM}(\Delta(x,y)) \mathbf{HWP} [22.5^\circ]$.

(ii) For rotations about a circular polarization axis, i.e., the $\hat{\mathbf{s}}_3$ axis, we can remove the half-wave plates, and use the sequence $\mathbf{R}_{\mathbf{s}_3}(\Delta(x,y)) = \mathbf{QWP} [-45^\circ] \mathbf{SLM}(\Delta(x,y)) \mathbf{QWP} [45^\circ]$. This sequence has been demonstrated to be particularly useful in creating vector beams such as radial and azimuthal polarization distributions [51]. For this, one begins with uniform horizontally polarized light, $\mathbf{E} = \hat{\mathbf{x}} = (\hat{\mathbf{i}} + \hat{\mathbf{r}}) / \sqrt{2}$. The right-circular component is retarded with respect to the

left-circular component resulting in the following polarization distribution after the waveplates and LC-SLM,

$$\mathbf{E} = \frac{1}{\sqrt{2}} \left(\hat{\mathbf{i}} + e^{i\Delta(x,y)} \hat{\mathbf{r}} \right) = \left(\cos \left(\frac{\Delta(x,y)}{2} \right) \hat{\mathbf{x}} - \sin \left(\frac{\Delta(x,y)}{2} \right) \hat{\mathbf{y}} \right) e^{i\Delta(x,y)/2}. \quad (6)$$

The polarization remains linear and is rotated in the laboratory by an angle of $\Delta(x,y)/2$. Thus, the linear polarization direction can vary spatially in an arbitrary manner. However, on the right side of Eq. (6) there appears an additional phase term that will not explicitly arise in our analysis using rotations in the Poincaré sphere. This phase is addressed in the Appendix B.

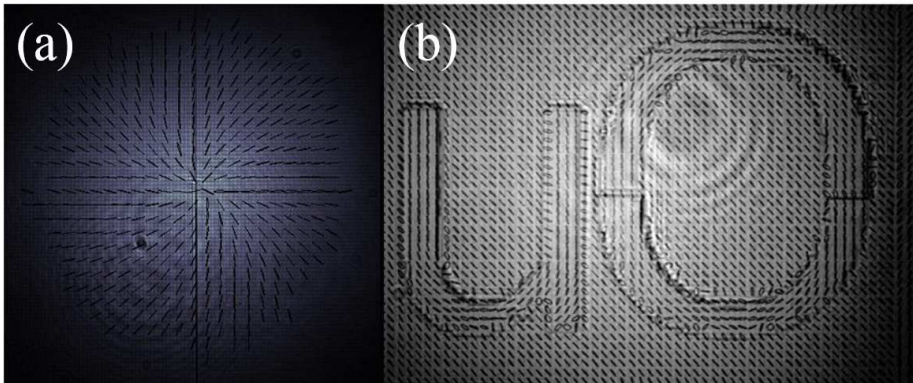


Figure 2: Arbitrary linear polarization rotations. (a) Rotations about $\hat{\mathbf{s}}_3$ axis to produce a radial polarization distribution. The black lines indicate the polarization direction, and the grey-scale gives the intensity. (b) This technique can be used to write arbitrary linear polarization patterns. Here, we write the initials of the University of Ottawa with polarization. See Appendix B for experimental details.

In Fig. 2(a) we demonstrate that the polarization can be aligned radially. In Fig. 2(b), the polarization follows the local asymptote of the letters “uO” (i.e., University of Ottawa). The presence of light at the center may seem surprising since radially polarized beams have a null in intensity at their center, as in a Laguerre-Gauss mode beam. However, in Fig. 2 we are imaging the LC-SLM surface, at which only the phase, rather than intensity is changed. The resulting field distribution is no longer a “beam” (for more detail on this subject see Appendix B).

3.3. Transformation from an arbitrary polarization state to another arbitrary polarization state

In our next step in increasing generality, we introduce a scheme to transform an arbitrary input polarization $\hat{\mathbf{s}}_i$ to another arbitrary output polarization, $\hat{\mathbf{s}}_o$. Both polarizations can spatially vary independently. Crucially, though, both $\hat{\mathbf{s}}_i$ and $\hat{\mathbf{s}}_o$ must be known at every position (x,y) before implementing the transformation, potentially through prior measurements.

To achieve this transformation, a second LC-SLM is added to the compound device of Eq. (5), thereby giving the ability to perform rotations about two distinct axes on the Poincaré sphere. Through two rotations about two orthogonal axes, say

$\hat{\mathbf{s}}_1$ and $\hat{\mathbf{s}}_2$, one can transform any point to any other point on the unit sphere [50]. However, this only holds if one can change the order of the orthogonal rotations, depending on the input and output states. In contrast, we consider a fixed ordering defined by the sequence of LC-SLMs and waveplates in the experimental setup.

In this section, it is useful to visualize the Poincaré sphere by projecting it on a plane spanned by our two rotation axes, $\hat{\mathbf{s}}_1$ and $\hat{\mathbf{s}}_2$. This is shown in Fig. 3(a). A rotation about $\hat{\mathbf{s}}_1$ will take $\hat{\mathbf{s}}_i$ to $\hat{\mathbf{s}}_m$. A following rotation about $\hat{\mathbf{s}}_2$ takes $\hat{\mathbf{s}}_m$ to $\hat{\mathbf{s}}_o$. Fig. 3(b) shows this sequence in a 3-dimensional view of the Poincaré sphere for reference. Reversing the order of the rotations would also work, but would instead pass through the intermediate state $\hat{\mathbf{s}}_{m'}$. This will not be generally true though. For many pairs of states $\hat{\mathbf{s}}_i$ and $\hat{\mathbf{s}}_o$, only one ordering will work. In particular, the region outlined in purple in Fig. 3(a) contains the subset of output states $\{\hat{\mathbf{s}}_o\}$ that can be reached from the specific $\hat{\mathbf{s}}_i$ when rotating about $\hat{\mathbf{s}}_1$ first, followed by $\hat{\mathbf{s}}_2$. To understand this, consider moving horizontally in either direction from $\hat{\mathbf{s}}_i$ along a line at $s_1^i = \hat{\mathbf{s}}_1 \cdot \hat{\mathbf{s}}_i$ (i.e., a rotation about $\hat{\mathbf{s}}_1$). In doing so, the largest achievable magnitude for $s_2^o = \hat{\mathbf{s}}_2 \cdot \hat{\mathbf{s}}_o$ is set by the intersection of the line with the circle bounding the Poincaré sphere. That is, at $1 = (s_1^i)^2 + (s_2^o)^2$.

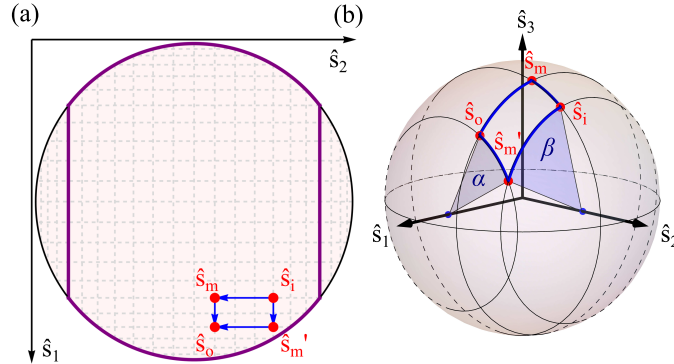


Figure 3: Representation of the transformation of an arbitrary polarization state $\hat{\mathbf{s}}_i$ into another arbitrary polarization state $\hat{\mathbf{s}}_o$ using 2 LC-SLMs. (a) represents the top view of the Poincaré Sphere depicted in (b). The input state $\hat{\mathbf{s}}_i$ can be converted to $\hat{\mathbf{s}}_o$ by a succession of one rotation about $\hat{\mathbf{s}}_1$ and one rotation about $\hat{\mathbf{s}}_2$. If the order of rotation is not defined, two intermediate points are possible: $\hat{\mathbf{s}}_m$ if the state is first rotated about $\hat{\mathbf{s}}_1$, and $\hat{\mathbf{s}}_{m'}$ if the state is first rotated about $\hat{\mathbf{s}}_2$. However, if the rotation about $\hat{\mathbf{s}}_1$ is the first one performed, then, there is only one possibility to go from $\hat{\mathbf{s}}_i$ to $\hat{\mathbf{s}}_o$, which means that it is impossible to reach any polarization state. In this case, the accessible states are in the region outlined in purple.

3.3.1. Required retardances Keeping this restriction in mind, we now calculate the required retardances, α and β , of the two LC-SLMs. We assume a configuration which rotates first about $\hat{\mathbf{s}}_1$ (by α) then $\hat{\mathbf{s}}_2$ (by β):

$$\mathbf{T}_{\mathbf{s}_i \rightarrow \mathbf{s}_o} = \mathbf{R}_{\mathbf{s}_2}(\beta)\mathbf{R}_{\mathbf{s}_1}(\alpha) = \mathbf{HWP}[112.5^\circ]\mathbf{SLM}(\beta)\mathbf{HWP}[22.5^\circ]\mathbf{SLM}(\alpha). \quad (7)$$

While for brevity we omit an explicit spatial dependence in these vectors and retardances, it should be understood to be implicit in what follows. Specifically, all

quantities are for the same transverse point in the light field. In order to transform an input polarization $\hat{\mathbf{s}}_i = [s_1^i, s_2^i, s_3^i]$ to a target output polarization $\hat{\mathbf{s}}_o = [s_1^o, s_2^o, s_3^o]$, one requires the following retardances:

$$\alpha' = \text{atan2} \left([0, s_2^i, s_3^i] \cdot [0, s_2^m, s_3^m], \text{sign}(s_2^i s_3^m - s_3^i s_2^m) \| [0, s_2^i, s_3^i] \times [0, s_2^m, s_3^m] \| \right), \quad (8)$$

$$\beta' = \text{atan2} \left([s_1^m, 0, s_3^m] \cdot [s_1^o, 0, s_3^o], \text{sign}(s_3^m s_1^o - s_1^m s_3^o) \| [s_1^m, 0, s_3^m] \times [s_1^o, 0, s_3^o] \| \right), \quad (9)$$

$$\hat{\mathbf{s}}_m = \left[s_1^i, s_2^o, \text{sign}(s_3^o) \sqrt{(s_3^i)^2 + (s_2^i)^2 - (s_2^o)^2} \right], \quad (10)$$

where $\hat{\mathbf{s}}_m = [s_1^m, s_2^m, s_3^m]$ is the intermediate point, \cdot is the dot product, \times is the vector cross product, $\|\hat{\mathbf{s}}\| = \sqrt{s_1^2 + s_2^2 + s_3^2}$ is the vector norm, and sign is the standard signum function. The function $\text{atan2}(x, y)$ is defined as the angle between the positive x axis and the point (x, y) , with angle increasing towards the positive y axis. Additionally, we take $\alpha = \alpha' + 2k\pi$ and $\beta = \beta' + 2k\pi$, in order to ensure that the two LC-SLMs rotate in the positive sense (the angle is increasing).

3.3.2. Applications of arbitrary to arbitrary polarization transformations We now present three examples of applications that use this transformation.

Ellipticity (de)magnifier: The ellipticity of an input state can be either magnified to be more circular, or demagnified to be more linear. In terms of the Poincaré sphere, changing the ellipticity of state $\hat{\mathbf{s}}_i$ corresponds to changing the input state's polar angle θ , while maintaining its azimuthal angle φ . This could be used to change a light field containing a spatial polarization distribution with an assortment of elliptical states to one with only linear states. It could also flip the polarization handedness. An example of the rotation paths is shown in Fig. (4).

Beam healer: Passage through birefringent optical media can undesirably transform a uniform polarization into a non-uniform polarization distribution. This effect could potentially degrade the performance of imaging systems. The method previously introduced in this section (i.e., Eq. (7)) can restore polarization uniformity. However, in order for the method to work for every polarization in the non-uniform distribution, the uniform output polarization must be either right or left-handed circular. In short, the transformation is $\mathbf{T}_{\mathbf{s}_i \rightarrow \pm \mathbf{s}_3}$.

While transforming an arbitrary polarization to another arbitrary polarization might seem completely general, it is not. We clarify this point in Appendix B.

3.4. Spatially variable retardation of a spatially variable polarization distribution

The most general polarization transformation is a rotation by an arbitrary angle ξ about an arbitrary axis $\hat{\mathbf{k}}$ in the Poincaré sphere, $\mathbf{R}_{\mathbf{k}}(\xi)$. This corresponds to a retardation of an arbitrary polarization state. It is a universal unitary transformation for polarization. The axis $\hat{\mathbf{k}}$ is defined by two free parameters, its spherical coordinates (φ, θ) , and rotation angle ξ adds a third parameter. It follows that one needs at least three control parameters in order to implement this general transformation. One solution is to use three variable liquid crystals and appropriate fixed waveplates. Considering LC-SLMs, this would implement a different general transformation at each and every transverse position in a light field.

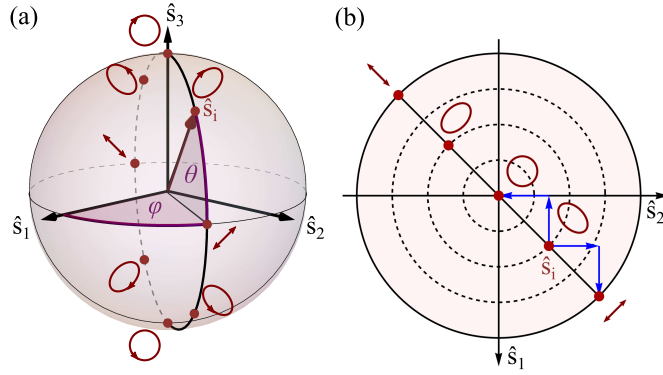


Figure 4: Representation of the action of a beam healer / beam ellipticity changer on the Poincaré Sphere. (b) represents the top view of the Poincaré Sphere depicted in (a). Here, an elliptical polarization state $\hat{\mathbf{s}}_i$, characterized by its coordinates ϕ and θ , can be transformed into any states laying on the great circle passing through the poles and itself using two LC-SLMs. In particular, the state $\hat{\mathbf{s}}_i$ can be converted to a linear state, in which case its ellipticity is removed, or converted into the state diametrically opposite on the Poincaré Sphere, in which case the sign of its ellipticity is flipped.

As in section 3.3, the LC-SLMs and waveplates effectively implement rotations about orthogonal axes. The addition of the third LC-SLM, and thus third rotation, allows us to draw upon the concept of proper extrinsic Euler angles, in which a general 3-d rotation $\mathbf{R}_{\mathbf{k}}(\xi)$ can be decomposed into three successive rotations about any two orthogonal axes. Here, we use $\hat{\mathbf{s}}_1$ and $\hat{\mathbf{s}}_2$. Accordingly, we compose the general rotation,

$$\begin{aligned}
 \mathbf{R}_{\mathbf{k}}(\xi) &= \mathbf{R}_{\hat{\mathbf{s}}_1}(\gamma)\mathbf{R}_{\hat{\mathbf{s}}_2}(\beta)\mathbf{R}_{\hat{\mathbf{s}}_1}(\alpha) \\
 &= \text{SLM}(\gamma)\text{HWP}[[112.5^\circ]]\text{SLM}(\beta)\text{HWP}[[22.5^\circ]]\text{SLM}(\alpha) \\
 &= \begin{bmatrix} \cos \beta & \sin \alpha \sin \beta & \cos \alpha \sin \beta \\ \sin \beta \sin \gamma & \cos \alpha \cos \gamma - \cos \beta \sin \alpha \sin \gamma & -\cos \gamma \sin \alpha - \cos \alpha \beta \sin \gamma \\ -\cos \gamma \sin \beta & \cos \beta \cos \gamma \sin \alpha + \cos \alpha \sin \gamma & \cos \alpha \cos \beta \cos \gamma - \sin \alpha \sin \gamma \end{bmatrix}.
 \end{aligned} \tag{11}$$

Fig. 5 demonstrates the sequential rotations that $\mathbf{R}_{\mathbf{k}}(\xi)$ performs on the principal axes in terms of the three angles α , β , and γ .

3.4.1. Required retardances To simplify our notation we write $\mathbf{R} \equiv \mathbf{R}_{\mathbf{k}}(\xi)$ in the following and define the \mathbf{R}_{ij} matrix element to be the i^{th} row from the top and j^{th} column from the left. In terms of these elements, the angle of each rotation is,

$$\alpha' = \text{atan2}(\mathbf{R}_{13}, \mathbf{R}_{12}), \tag{12}$$

$$\beta' = \text{atan2}(\mathbf{R}_{11}, \sqrt{\mathbf{R}_{21}^2 + \mathbf{R}_{31}^2}), \tag{13}$$

$$\gamma' = \text{atan2}(-\mathbf{R}_{31}, \mathbf{R}_{21}). \tag{14}$$

These angles, modded by 2π , are the retardances, α , β , and γ , that are applied at each transverse position in the light field by the three LC-SLMs.

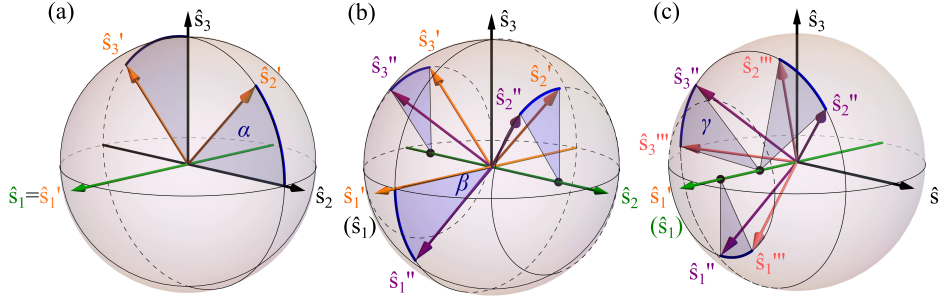


Figure 5: Creation of a general unitary transformation using a sequence of three orthogonal Euler rotations. The first rotation (a) is about $\hat{\mathbf{s}}_1$ by angle α , the second (b) about $\hat{\mathbf{s}}_2$ by β , and the third (c) about $\hat{\mathbf{s}}_1$ by γ . From the transformation of the main axes of the Poincaré Sphere (e.g., $\hat{\mathbf{s}}_1 \rightarrow \hat{\mathbf{s}}_1' \rightarrow \hat{\mathbf{s}}_1'' \rightarrow \hat{\mathbf{s}}_1'''$) one can see that this combination of rotations performs a general 3d rotation (e.g., yaw, pitch, and roll), and, consequently, a general polarization rotation up to a global phase.

These angles are sufficient if one begins with the actual matrix for $\mathbf{R}_{\mathbf{k}}(\xi)$, but it may be more useful if they are expressed in terms of the rotation axis $\hat{\mathbf{k}} = [k_1, k_2, k_3]$ and angle ξ ,

$$\alpha' = \frac{k_1 k_2 (1 - \cos \xi) - k_3 \sin \xi}{k_2 \sin \xi + k_1 k_3 (1 - \cos \xi)}, \quad (15)$$

$$\beta' = \frac{[(k_3 \sin \xi + k_1 k_2 (1 - \cos \xi))^2 + (k_1 k_3 (1 - \cos \xi) - k_2 \sin \xi)^2]^{1/2}}{\cos \xi + k_1^2 (1 - \cos \xi)}, \quad (16)$$

$$\gamma' = \frac{k_3 \sin \xi + k_1 k_2 (1 - \cos \xi)}{-(k_1 k_3 (1 - \cos \xi) - k_2 \sin \xi)}. \quad (17)$$

These follow from the matrix expression of the Euler-Rodrigues formula, Eq. (25) and Eq. (12)-(14). With these retardances, a completely general polarization unitary can be applied at each transverse position (x, y) in a light field.

3.4.2. Applications and examples Compensation of arbitrary spatially dependent birefringence: Now that we are able to implement a fully universal polarization transformation, we can fully compensate for propagation through optical media. For example, in propagation through a multi-mode optical fiber, stresses and strains in the fiber typically create a small local birefringence that effects supported modes differently. This leads to a spatially dependent unitary $\mathbf{R} \equiv \mathbf{R}_{\mathbf{k}}(\xi)$. If one is attempting to use spatial and polarization multiplexing to communicate over such a fiber, this unwanted transformation will cause cross-talk and errors.

Spatially resolved polarization tomography can determine $\mathbf{R}_{\mathbf{k}(x,y)}(\xi(x,y))$ for the fiber. Once this is known, the apparatus described in this section could be placed after the fiber to implement $\mathbf{R}_{\mathbf{k}(x,y)}(-\xi(x,y))$, thereby undoing the transformation. Every spatial mode would emerge with the same polarization that it had at the fiber input.

4. Conclusion

In order to completely control photons and unlock their full potential, scientists must be able to arbitrarily manipulate all four degrees of freedom that fully describe their state: time-frequency, the two transverse position-momentum directions (e.g., x and y), and polarization. In this paper, we described in detail methods to manipulate polarization with liquid crystal devices in conjunction with fixed waveplates. Most generally, we showed how to implement any possible polarization transformation, a universal unitary. Since they are based on liquid crystals, these unitaries can be varied or even completely reconfigured in milliseconds and be computer controlled. Faster operation (e.g., sub-nanosecond) can be achieved by instead using an electro-optic phase modulator [52], which retards light in a similar manner to a liquid crystal.

Combining these methods with spatial light modulators allows for novel and broad control of the spatially varying polarizations of light-fields. Beyond producing vector polarized beams, we proposed a number of applications of these transformations including repairing polarization aberrations in a beam, as a polarization magnifier, and for the compensation of spatial-mode dependent birefringence in fiber-optic communications. Given the broad use of polarization in industrial processes, commercial products, and scientific research, we expect that these general polarization methods will have many more applications in the near future.

Funding

This research was undertaken, in part, thanks to funding from the Canada Research Chairs, NSERC Discovery, Canada Foundation for Innovation, and the Canada Excellence Research Chairs program.

Appendix A: Polarization conventions and transformations

In this section, we give a brief theoretical review of polarization manipulation. The reader should be aware that there are many conflicting conventions in use for polarization. This section presents a consistent set of definitions (see Table 1 for a summary) with which to apply the schemes we introduce in the main text. We characterize the polarization by the manner in which the electric field oscillates. That is, by the normalized complex vector,

$$\mathbf{E} = a_x \hat{\mathbf{x}} + a_y e^{i\delta} \hat{\mathbf{y}}, \quad (18)$$

where a_x and a_y are the amplitudes of, and δ the relative phase between, the x and y electric field components, respectively, with $a_x^2 + a_y^2 = 1$. With $\hat{\mathbf{z}}$ pointing in the direction of propagation, we use a right-handed co-ordinate system. We follow the convention in Ref. [49] by defining right-handed polarization to be clockwise rotating, as seen by the receiver. When $\delta \neq k\pi/2$, where k is an integer, the polarization state is “elliptical” since the electric field vector traces out an ellipse as a function of time.

A visually intuitive representation for polarization states is to represent them as points on the surface of a unit sphere, known as the Poincaré sphere [5], as shown in Fig. 6(a), the polarization equivalent of the Bloch sphere for spin-1/2 or other two-level systems. From the complex vector notation, we can calculate the reduced (normalized) Stokes parameters [5] to obtain a polarization state’s position on the

sphere,

$$s_0 = E_x E_x^* + E_y E_y^* = a_x^2 + a_y^2 = 1, \quad (19)$$

$$s_1 = E_x E_x^* - E_y E_y^* = a_x^2 - a_y^2 = \cos \varphi \cos \theta, \quad (20)$$

$$s_2 = E_x E_y^* + E_y E_x^* = 2a_x^2 a_y^2 \cos \delta = \sin \varphi \cos \theta, \quad (21)$$

$$s_3 = i(E_x E_y^* - E_y E_x^*) = 2a_x^2 a_y^2 \sin \delta = \sin \theta, \quad (22)$$

where φ and θ are the azimuthal and polar angles of the Poincaré sphere. Here, we consider left- and right-handed circular polarizations are respectively mapped to the north and south poles of the sphere. Linear polarization states lie along the equator and elliptical states everywhere else. Orthogonal polarization states are diametrically opposed points. The six polarizations that define the axes are listed in Table 1.

Polarization state	Abbrev.	Laboratory		Poincaré Sphere	
		Vector	Ellipse	Stokes vector $\hat{\mathbf{s}}$	(φ, θ)
Horizontal	H	$\hat{\mathbf{x}}$	—	$[1, 0, 0]$	$(0, 0)$
Vertical	V	$\hat{\mathbf{y}}$		$[-1, 0, 0]$	$(\pi, 0)$
Diagonal	D	$\hat{\mathbf{d}} = \frac{(\hat{\mathbf{x}} + \hat{\mathbf{y}})}{\sqrt{2}}$	/	$[0, 1, 0]$	$(\pi/2, 0)$
Anti-Diagonal	A	$\hat{\mathbf{a}} = \frac{(\hat{\mathbf{x}} - \hat{\mathbf{y}})}{\sqrt{2}}$	\	$[0, -1, 0]$	$(-\pi/2, 0)$
Right-Hand Circular	R	$\hat{\mathbf{r}} = \frac{(\hat{\mathbf{x}} + i\hat{\mathbf{y}})}{\sqrt{2}}$	⊙	$[0, 0, 1]$	$(0, \pi/2)$
Left-Hand Circular	L	$\hat{\mathbf{l}} = \frac{(\hat{\mathbf{x}} - i\hat{\mathbf{y}})}{\sqrt{2}}$	⊙	$[0, 0, -1]$	$(0, -\pi/2)$

Table 1: Table of the conventions used through this paper to define the principal polarization states (i.e the main axes of the Poincaré sphere), their abbreviations and their representations both in the laboratory frame and on the Poincaré sphere. For the pictorial representation in the Ellipse column, the direction of propagation is towards the observer.

In this paper, we consider only completely polarized states of light. Consequently, the length of the reduced Stokes vector, defined by s_0 , is identically one, such that all states lie on the surface of the Poincaré sphere. Henceforth, we drop s_0 so that a polarization state is described by a three element Stokes vector $\hat{\mathbf{s}} = s_1 \hat{\mathbf{s}}_1 + s_2 \hat{\mathbf{s}}_2 + s_3 \hat{\mathbf{s}}_3 = [s_1, s_2, s_3]$. Alternately, this unit vector can be equivalently expressed in spherical coordinates as $\hat{\mathbf{s}}(\varphi, \theta)$. The angles φ and θ can be related to the complex vector notation via,

$$\sin \varphi = 2a_x^2 a_y^2 \sin \delta, \quad (23)$$

$$\tan \theta = \frac{2a_x^2 a_y^2 \sin \delta}{\sqrt{(a_x^2 - a_y^2)^2 + 4a_x^4 a_y^4 \cos^2 \delta}}. \quad (24)$$

In terms of these parameters, we use the conventions listed in Table 1.

As shown in Fig. 6(b), on the Poincaré sphere, polarization transformations — general polarization unitaries — are right-handed rotations of a state $\hat{\mathbf{s}}$ about a unit-length axis $\hat{\mathbf{k}} = [k_1, k_2, k_3] = \hat{\mathbf{k}}(\varphi, \theta)$ by an angle ξ . Mathematically, to perform such a rotation on a Stokes vector, we use a standard three-dimensional *active* rotation matrix, $\mathbf{R}_{\mathbf{k}}(\xi)$. These 3×3 matrices are simply the lower-right sub-matrix of the 4×4 Mueller rotation matrices used commonly in polarization theory. Using this matrix

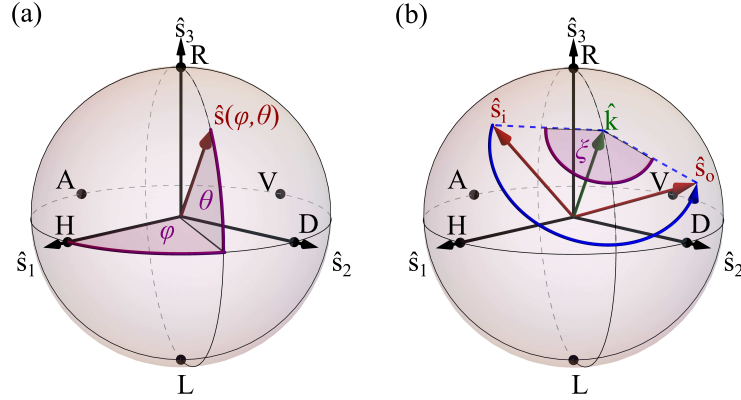


Figure 6: The Poincaré sphere and polarization transformations. Polarization states lie on the surface of a sphere that has a radius of one. Horizontal (H) and vertical (V) polarizations define the \hat{s}_1 axis, diagonal (D) and anti-diagonal (A) states define the \hat{s}_2 axis, and left- (L) and right-hand (R) circular define the polar \hat{s}_3 axis; each pair lie on the positive and negative ends of the axis, respectively. (a) The polarization state in Eq. (18) is given by point $\hat{\mathbf{s}}(\varphi, \theta) = [s_1, s_2, s_3]$ on the surface, where s_i are the Stokes parameters. The polarization state $\hat{\mathbf{s}}$ can also be expressed by its coordinates in the spherical system $\hat{\mathbf{s}}(\varphi, \theta)$. (b) In a polarization transformation, any polarization state is rotated about a fixed axis $\hat{\mathbf{k}}$ by an angle ξ . *Note: Throughout this paper, the states are represented in red, the axes of rotation in green, the transformation in blue and the definition of angle in purple.*

and writing the Stokes vector as a column, the rotated vector is $\hat{\mathbf{s}}' = \mathbf{R}_{\mathbf{k}}(\xi)\hat{\mathbf{s}}$. The general rotation matrix $\mathbf{R}_{\mathbf{k}}(\xi)$ is given by a form of the Euler-Rodrigues formula [50],

$$\mathbf{R}_{\mathbf{k}}(\xi) = \mathbf{I} + \sin \xi \mathbf{K} + (1 - \cos \xi) \mathbf{K}^2, \quad (25)$$

where \mathbf{I} is the 3×3 identity matrix, and \mathbf{K} is the cross-product operation matrix of $\hat{\mathbf{k}}$,

$$\hat{\mathbf{k}} \times = \mathbf{K} = \begin{bmatrix} 0 & -k_3 & k_2 \\ k_3 & 0 & -k_1 \\ -k_2 & k_1 & 0 \end{bmatrix}. \quad (26)$$

This gives a rotation matrix of,

$$\mathbf{R}_{\mathbf{k}}(\xi) = \begin{bmatrix} \cos \xi + k_1^2(1 - \cos \xi) & k_1 k_2(1 - \cos \xi) - k_3 \sin \xi & k_1 k_3(1 - \cos \xi) + k_2 \sin \xi \\ k_1 k_2(1 - \cos \xi) + k_3 \sin \xi & \cos \xi + k_2^2(1 - \cos \xi) & k_2 k_3(1 - \cos \xi) - k_1 \sin \xi \\ k_1 k_3(1 - \cos \xi) - k_2 \sin \xi & k_2 k_3(1 - \cos \xi) + k_1 \sin \xi & \cos \xi + k_3^2(1 - \cos \xi) \end{bmatrix}. \quad (27)$$

The rotation matrices for rotations about the \hat{s}_1 , \hat{s}_2 , and \hat{s}_3 axes can thus be

computed from Eq. (27) using $\hat{\mathbf{k}} = [1, 0, 0]$, $[0, 1, 0]$, and $[0, 0, 1]$, respectively,

$$\mathbf{R}_{\mathbf{s}_1}(\alpha) = \begin{bmatrix} 1 & 0 & 0 \\ 0 & \cos \alpha & -\sin \alpha \\ 0 & \sin \alpha & \cos \alpha \end{bmatrix}, \quad (28)$$

$$\mathbf{R}_{\mathbf{s}_2}(\beta) = \begin{bmatrix} \cos \beta & 0 & \sin \beta \\ 0 & 1 & 0 \\ -\sin \beta & 0 & \cos \beta \end{bmatrix}, \quad (29)$$

$$\mathbf{R}_{\mathbf{s}_3}(\gamma) = \begin{bmatrix} \cos \gamma & -\sin \gamma & 0 \\ \sin \gamma & \cos \gamma & 0 \\ 0 & 0 & 1 \end{bmatrix}. \quad (30)$$

Appendix B: Residual Spatial Phase, Relay Imaging, and non-Universal Transformations

In this paper, we concern ourselves only with the the spatial polarization distribution of the beam and neglect spatially varying phases. Nonetheless, the two are linked. There are three physical phases, δ , b , and c , in a single frequency paraxial optical field, $\mathbf{E}(x, y) = (a_x \hat{\mathbf{x}} + a_y e^{i\delta(x, y)} \hat{\mathbf{y}}) e^{ib(x, y)} e^{ic}$. Phase c is an overall global phase that is constant across x and y , and, hence, not relevant for this paper (it is relevant for interference with ancillary fields, as in an interferometer). Phase $b(x, y)$ is between fields at different positions. Phase $\delta(x, y)$ is between field polarization components at (x, y) and can vary with x and y . It is this last phase, as well as the magnitude of each polarization component, that we manipulate in this paper.

Residual Phase

However, a residual spatially-varying phase $b(x, y)$ can indeed arise in the polarization transformations that we present. This phase is not evident from rotations in the Poincaré sphere but does arise when using Jones Matrices [48]. At the expense of added complexity, one could compensate for $b(x, y)$ by adding one additional LC-SLM to each of the transformations presented. If not compensated, this residual phase can have physical consequences. As an example, consider the case where we produce a radially polarized field according to Eq. (6). On the right-hand side, a residual phase of $e^{i\Delta(x, y)}$ appears. Here, $\Delta(x, y) = 2\phi$, where ϕ is the azimuthal angle about the center of the radial field. It's impact can be understood by considering the left-hand side of Eq. (6), $\mathbf{E} = \frac{1}{\sqrt{2}} (\hat{\mathbf{i}} + e^{i2\phi} \hat{\mathbf{r}})$. If an incoming optical field had a Gaussian transverse profile, the left-handed component $\hat{\mathbf{i}}$ would be unchanged, whereas the right-handed component $\hat{\mathbf{r}}$ would receive an azimuthally-varying phase carrying $\ell = 2$ units of orbital angular momentum (OAM). This phase profile causes the right-handed light-field to no longer be a solution to the paraxial wave equation. Hence, it is no longer a “beam” in the sense that it does not maintain its spatial and polarization distribution upon propagation (up to a scale factor). We experimentally demonstrated this by allowing the radial field in Fig. 7(a) to propagate 10 cm further. The polarization and intensity distribution at this point is shown in Fig. 7(b). We call this the “far-field”.

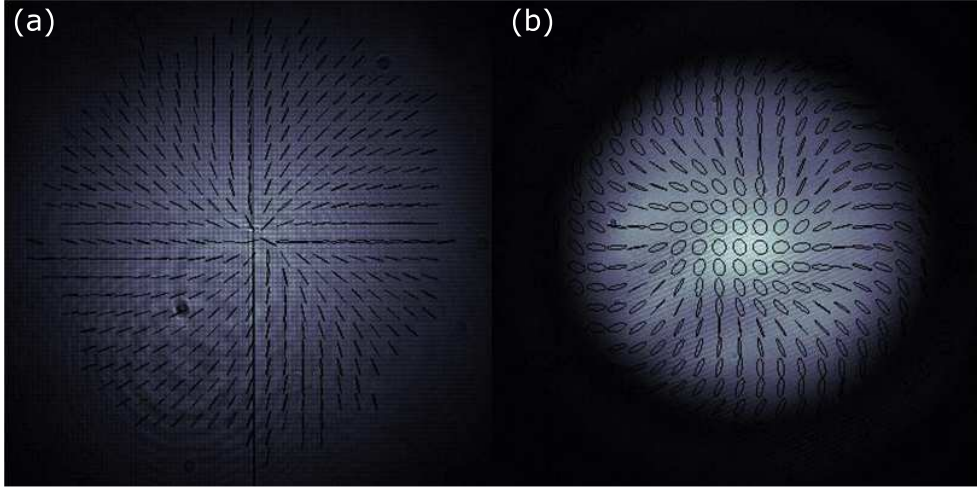


Figure 7: Rotations about $\hat{\mathbf{s}}_3$ axis to produce radial polarization distribution. We can see the pictures of the beam and its polarization state at various positions in the imaging plane (a) and "far-field" (b).

Imaging requirements for general polarization manipulation

Fig. 2 shows there are notable differences between the output polarization distribution at the image plane of the LC-SLM (near-field) and after propagation (far-field) for the same input polarization and LC-SLM phase pattern, $\Delta(x, y)$. However, throughout this paper we assumed that LC-SLMs can be placed in series while acting on the same unchanged optical field. To achieve this, the field at one LC-SLM is imaged onto the next with a 4-f system. The latter acts as a relay imaging system with a one-to-one magnification ratio.

Ideally, in order to create a simple setup with high transmissivity, the LC-SLMs would be transmissive and placed in a line. However, reflective LC-SLMs often have better performance specifications. A reflective setup usually involves picking off a beam that is reflected at a small angle. Since, the pick-off mirror acts as an aperture this can dramatically change the optical field imaged by a 4-f setup. Our setup, shown in Fig. 8, uses a reflective LC-SLM. In order to separate the reflected beam from incident beam we use a non-polarizing beam-splitter (NPBS) instead of a pick-off mirror. The drawback is that this NPBS introduces loss. Nonetheless, the setup allows us to test the transformations, which are lossless in principle.

Arbitrary to arbitrary polarization versus universal transformations

While transforming an arbitrary polarization to another arbitrary polarization might seem completely general, it is not. The most general rotation is $\mathbf{R}_{\mathbf{k}}(\xi)$, whereas the transformation that is implemented through this method is $\mathbf{R}_{\mathbf{s}_2}(\beta)\mathbf{R}_{\mathbf{s}_1}(\alpha)$. The latter implements $\mathbf{T}_{\mathbf{s}_i \rightarrow \mathbf{s}_o}$, which takes $\hat{\mathbf{s}}_i \rightarrow \hat{\mathbf{s}}_o$. It also links the polarization states diametrically opposed to these on the Poincaré sphere, $-\hat{\mathbf{s}}_i \rightarrow -\hat{\mathbf{s}}_o$. However, $\mathbf{T}_{\mathbf{s}_i \rightarrow \mathbf{s}_o}$ does not fix the retardance ζ between $\hat{\mathbf{s}}_o$ and $-\hat{\mathbf{s}}_o$. This retardance is crucial when considering how $\mathbf{T}_{\mathbf{s}_i \rightarrow \mathbf{s}_o}$ transforms any input state other than $\pm\hat{\mathbf{s}}_i$. Polarizations that are a superposition of $-\hat{\mathbf{s}}_o$ and $+\hat{\mathbf{s}}_o$ will transform in an undetermined way.

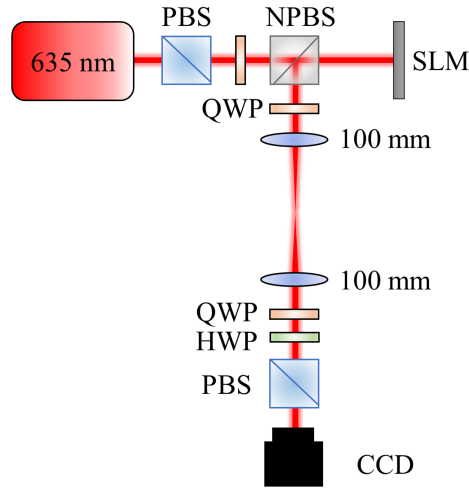


Figure 8: Experimental setup to perform a rotation about \hat{s}_3 . A diode laser (635 nm) is prepared to be left-handed circular with a quarter-wave plate (QWP), and then reflected off of an LC-SLM (LCOS-SLM X10468, Hamamatsu, Japan), which imprints the desired spatially varying phase (i.e., rotation angle or “retardance”). A non-polarizing beam-splitter (NPBS) splits off half of the light to be analyzed. A second quarter-wave plate converts circular states back to linear states. A 4-f imaging system is used to image the plane of the LC-SLM onto a CCD camera. We use short focal length ($f = 100$ mm, diameter = 25.4 mm) doublet lenses in order to have a high numerical aperture. The polarization of the light is then determined pixel by pixel via polarization tomography (i.e., Stokes polarimetry) with a half-wave plate (HWP), quarter-wave plate, and polarizing beam-splitter (PBS) [53].

References

- [1] R. Bhandari, “Synthesis of general polarization transformers. A geometric phase approach,” *Physics Letters A* **138**, 469–473 (1989).
- [2] R. Simon and N. Mukunda, “Minimal three-component $SU(2)$ gadget for polarization optics,” *Physics Letters A* **143**, 165–169 (1990).
- [3] J. N. Damask, *Polarization optics in telecommunications*, vol. 101 (Springer Science & Business Media, 2004).
- [4] F. De Zela, “Two-component gadget for transforming any two nonorthogonal polarization states into one another,” *Physics Letters A* **376**, 1664–1668 (2012).
- [5] M. Born and E. Wolf, *Principles of optics: electromagnetic theory of propagation, interference and diffraction of light* (Elsevier, 1980).
- [6] T. W. Clark, R. F. Offer, S. Franke-Arnold, A. S. Arnold, and N. Radwell, “Comparison of beam generation techniques using a phase only spatial light modulator,” *Optics express* **24**, 6249–6264 (2016).
- [7] E. Bolduc, N. Bent, E. Santamato, E. Karimi, and R. W. Boyd, “Exact solution to simultaneous intensity and phase encryption with a single phase-only hologram,” *Optics Letters* **38**, 3546–3549 (2013).
- [8] V. Arrizón, U. Ruiz, R. Carrada, and L. A. González, “Pixelated phase computer holograms for the accurate encoding of scalar complex fields,” *JOSA A* **24**, 3500–3507 (2007).
- [9] M. A. A. Neil, F. Massoumian, R. Juškaitis, and T. Wilson, “Method for the generation of arbitrary complex vector wave fronts,” *Opt. Lett.* **27**, 1929–1931 (2002).
- [10] C. Maurer, A. Jesacher, S. Fürhapter, S. Bernet, and M. Ritsch-Marte, “Tailoring of arbitrary optical vector beams,” *New Journal of Physics* **9**, 78 (2007).

- [11] X.-L. Wang, J. Ding, W.-J. Ni, C.-S. Guo, and H.-T. Wang, "Generation of arbitrary vector beams with a spatial light modulator and a common path interferometric arrangement," *Opt. Lett.* **32**, 3549–3551 (2007).
- [12] S. Franke-Arnold, J. Leach, M. J. Padgett, V. E. Lembessis, D. Ellinas, A. J. Wright, J. M. Girkin, P. Öhberg, and A. S. Arnold, "Optical ferris wheel for ultracold atoms," *Opt. Express* **15**, 8619–8625 (2007).
- [13] H. Chen, J. Hao, B.-F. Zhang, J. Xu, J. Ding, and H.-T. Wang, "Generation of vector beam with space-variant distribution of both polarization and phase," *Opt. Lett.* **36**, 3179–3181 (2011).
- [14] I. Moreno, J. A. Davis, T. M. Hernandez, D. M. Cottrell, and D. Sand, "Complete polarization control of light from a liquid crystal spatial light modulator," *Opt. Express* **20**, 364–376 (2012).
- [15] W. Han, Y. Yang, W. Cheng, and Q. Zhan, "Vectorial optical field generator for the creation of arbitrarily complex fields," *Optics Express* **21**, 20692 (2013).
- [16] E. H. Waller and G. von Freymann, "Independent spatial intensity, phase and polarization distributions," *Optics Express* **21**, 28167 (2013).
- [17] D. Maluenda, I. Juvells, R. Martínez-Herrero, and A. Carnicer, "Reconfigurable beams with arbitrary polarization and shape distributions at a given plane," *Opt. Express* **21**, 5432–5439 (2013).
- [18] C.-S. Guo, Z.-Y. Rong, and S.-Z. Wang, "Double-channel vector spatial light modulator for generation of arbitrary complex vector beams," *Opt. Lett.* **39**, 386 (2014).
- [19] Z. Yu, H. Chen, Z. Chen, J. Hao, and J. Ding, "Simultaneous tailoring of complete polarization, amplitude and phase of vector beams," *Opt. Commun.* **345**, 135–140 (2015).
- [20] D. Walls and G. Milburn, *Quantum Optics*, SpringerLink: Springer e-Books (Springer Berlin Heidelberg, 2008).
- [21] J. A. Davis, D. E. McNamara, D. M. Cottrell, and T. Sonehara, "Two-dimensional polarization encoding with a phase-only liquid-crystal spatial light modulator," *Appl. Opt.* **39**, 1549–1554 (2000).
- [22] R. L. Eriksen, P. C. Mogensen, and J. Glückstad, "Elliptical polarisation encoding in two dimensions using phase-only spatial light modulators," *Opt. Commun.* **187**, 325–336 (2001).
- [23] F. Kenny, D. Lara, O. G. Rodríguez-Herrera, and C. Dainty, "Complete polarization and phase control for focus-shaping in high-na microscopy," *Opt. Express* **20**, 14015–14029 (2012).
- [24] I. Estévez, A. Lizana, X. Zheng, A. Peinado, C. Ramírez, J. L. Martínez, A. Márquez, I. Moreno, and J. Campos, "Parallel aligned liquid crystal on silicon display based optical set-up for the generation of polarization spatial distributions," in "Modeling Aspects in Optical Metrology V," B. Bodermann, K. Frenner, and R. M. Silver, eds. (SPIE-Intl Soc Optical Eng, 2015), p. 95261A.
- [25] X. Zheng, A. Lizana, A. Peinado, C. Ramirez, J. L. Martinez, A. Marquez, I. Moreno, and J. Campos, "Compact lcos - slm based polarization pattern beam generator," *Journal of Lightwave Technology* **33**, 2047–2055 (2015).
- [26] E. J. Galvez, S. Khadka, W. H. Schubert, and S. Nomoto, "Poincaré-beam patterns produced by nonseparable superpositions of laguerre-gauss and polarization modes of light," *Applied optics* **51**, 2925–2934 (2012).
- [27] I. Freund, M. S. Soskin, R. I. Egorov, and V. Denisenko, "Diabolo creation and annihilation," *Optics letters* **31**, 2381–2383 (2006).
- [28] F. Cardano, E. Karimi, L. Marrucci, C. de Lisio, and E. Santamato, "Generation and dynamics of optical beams with polarization singularities," *Optics express* **21**, 8815–8820 (2013).
- [29] B. Khajavi and E. Galvez, "High-order disclinations in space-variant polarization," *Journal of Optics* **18**, 084003 (2016).
- [30] E. Otte, C. Alpmann, and C. Denz, "Higher-order polarization singularities in tailored vector beams," *Journal of Optics* **18**, 074012 (2016).
- [31] S. K. Pal and P. Senthilkumaran, "Cultivation of lemon fields," *Optics Express* **24**, 28008–28013 (2016).
- [32] T. Bauer, P. Banzer, E. Karimi, S. Orlov, A. Rubano, L. Marrucci, E. Santamato, R. W. Boyd, and G. Leuchs, "Observation of optical polarization möbius strips," *Science* **347**, 964–966 (2015).
- [33] K. Dholakia and T. Čižmár, "Shaping the future of manipulation," *Nature Photonics* **5**, 335–342 (2011).
- [34] J. Leach, H. Mushfique, R. di Leonardo, M. Padgett, and J. Cooper, "An optically driven pump for microfluidics," *Lab on a Chip* **6**, 735–739 (2006).
- [35] J.-P. Delville, M. R. de Saint Vincent, R. D. Schroll, B. Issenmann, D. Lasseux, W. W. Zhang,

- E. Brasselet, "Laser microfluidics: fluid actuation by light," *Journal of Optics A: Pure and Applied Optics* **11**, 034015 (2009).
- [36] M. Schadt, K. Schmitt, V. Kozinkov, and V. Chigrinov, "Surface-induced parallel alignment of liquid crystals by linearly polymerized photopolymers," *Japanese Journal of Applied Physics* **31**, 2155 (1992).
- [37] A. Ambrosio, L. Marrucci, F. Borbone, A. Roviello, and P. Maddalena, "Light-induced spiral mass transport in azo-polymer films under vortex-beam illumination," *Nature communications* **3**, 989 (2012).
- [38] K. Toyoda, F. Takahashi, S. Takizawa, Y. Tokizane, K. Miyamoto, R. Morita, and T. Omatsu, "Transfer of light helicity to nanostructures," *Physical review letters* **110**, 143603 (2013).
- [39] G. Milione, T. A. Nguyen, E. Karimi, D. A. Nolan, S. Slussarenko, L. Marrucci, and R. Alfano, "Superdense coding with vector vortex beams: A classical analogy of entanglement," in "Frontiers in Optics 2013," (Optical Society of America, 2013), p. FM3F.4.
- [40] P. Li, Y. Sun, Z. Yang, X. Song, and X. Zhang, "Classical hypercorrelation and wave-optics analogy of quantum superdense coding," *Scientific reports* **5**, 18574 (2015).
- [41] E. Karimi, J. Leach, S. Slussarenko, B. Piccirillo, L. Marrucci, L. Chen, W. She, S. Franke-Arnold, M. J. Padgett, and E. Santamato, "Spin-orbit hybrid entanglement of photons and quantum contextuality," *Phys. Rev. A* **82**, 022115 (2010).
- [42] E. Karimi, F. Cardano, M. Maffei, C. de Lisio, L. Marrucci, R. W. Boyd, and E. Santamato, "Hardy's paradox tested in the spin-orbit hilbert space of single photons," *Physical Review A* **89**, 032122 (2014).
- [43] G. Vallone, V. D'Ambrosio, A. Sponselli, S. Slussarenko, L. Marrucci, F. Sciarrino, and P. Villoresi, "Free-space quantum key distribution by rotation-invariant twisted photons," *Phys. Rev. Lett.* **113**, 060503 (2014).
- [44] A. Sit, F. Bouchard, R. Fickler, J. Gagnon-Bischoff, H. Larocque, K. Heshami, D. Elser, C. Peuntinger, K. Günthner, B. Heim, C. Marquardt, G. Leuchs, R.W. Boyd, "High-dimensional intra-city quantum cryptography with structured photons," arXiv preprint arXiv:1612.05195 (2016).
- [45] B. Ndagano, B. Perez-Garcia, F. S. Roux, M. McLaren, C. Rosales-Guzman, Y. Zhang, O. Mouane, R. I. Hernandez-Aranda, T. Konrad, and A. Forbes, "Characterizing quantum channels with non-separable states of classical light," *Nature Physics* (2017).
- [46] F. Töppel, A. Aiello, C. Marquardt, E. Giacobino, and G. Leuchs, "Classical entanglement in polarization metrology," *New Journal of Physics* **16**, 073019 (2014).
- [47] S. Berg-Johansen, F. Töppel, B. Stiller, P. Banzer, M. Ornigotti, E. Giacobino, G. Leuchs, A. Aiello, and C. Marquardt, "Classically entangled optical beams for high-speed kinematic sensing," *Optica* **2**, 864–868 (2015).
- [48] R. C. Jones, "A new calculus for the treatment of optical systems," *J. Opt. Soc. A* **37**, 110–112 (1947).
- [49] B. Saleh and M. Teich, *Fundamentals of Photonics*, Wiley Series in Pure and Applied Optics (Wiley, 2013).
- [50] D. Koks, *Explorations in Mathematical Physics: The Concepts Behind an Elegant Language* (Springer New York, 2006), chap. 4, p. 147, SpringerLink: Springer e-Books.
- [51] Z. Zhuang, Y. J. Kim, and J. S. Patel, "Electrically controllable azimuth optical rotator," *Appl. Phys. Lett.* **76**, 2334 (2000).
- [52] A. Yariv and P. Yeh, *Photonics: Optical Electronics in Modern Communications* (Oxford University Press, 2007), chap. 9, p. 418, The Oxford series in electrical and computer engineering.
- [53] F. Cardano, E. Karimi, S. Slussarenko, L. Marrucci, C. de Lisio, and E. Santamato, "Polarization pattern of vector vortex beams generated by q-plates with different topological charges," *Applied optics* **51**, C1–C6 (2012).